FEDERAL UNIVERSITY OF TECHNOLOGY, AKURE
JOURNAL OF ENGINEERING AND ENGINEERING TECHNOLOGY

MACHINE LEARNING OPTIMIZATION OF UNDERFILL FLOW TIME IN FLIP-CHIP ENCAPSULATION OF BGA ASSEMBLIES

[1]Apalowo, R. K.*, [1]Kehinde, J. I., [1]Oyeleke, E. O., [1]Owoloja, O. J. and [1]Famuyiwa, S. O.

[1]Department of Mechanical Engineering, Federal University of Technology, Akure, Ondo State, Nigeria

**Corresponding author: rkapalowo@futa.edu.ng*

Apalowo R. K., Kehinde J. I., Oyeleke E. O., Owoloja O. J., Famuyiwa S. O. (2026): Machine Learning Optimization of Underfill Flow Time in Flip-Chip Encapsulation of BGA Assemblies, 20 (1) 8-20

Received Date: 15.01.2026 **Accepted Date: 10.03.2026**

Abstract
Predicting and minimizing underfill flow time remains challenging due to complex nonlinear interactions among material properties, solder bump geometry, and dispensing strategy. This study presents a hybrid computational framework integrating computational fluid dynamics (CFD) simulations with machine learning–based predictive modeling to analyze and optimize underfill flow behavior. A total of 120 simulations were performed using ANSYS Fluent, covering six dispensing configurations, four solder bump geometries (spherical, cylindrical, hourglass, and concave), and five underfill materials with varying viscosity, surface tension, and density. To eliminate volumetric bias, an inlet-area-balanced dispensing strategy was implemented to maintain constant total injection volume across configurations. Taguchi-based parametric analysis revealed that underfill material viscosity is the dominant factor governing flow time, followed by dispensing configuration, while bump geometry shows comparatively minor influence. Bayesian optimization using Scikit-Optimize and Optuna identified the optimal configuration as hourglass-shaped solder bumps, U-33.3 three-inlet dispensing, and a low-viscosity methanol-based underfill. Among the evaluated machine learning models, Random Forest achieved the highest predictive accuracy (RMSE = 1.19), demonstrating strong capability in modeling nonlinear process interactions and enabling data-driven optimization of encapsulation processes. The CFD–ML framework provides a computationally efficient tool for encapsulation process optimization, enabling accelerated virtual prototyping and data-driven design in microelectronic packaging.

Keywords: *Flip-chip BGA packaging, Underfill encapsulation, Capillary flow dynamics, Machine learning optimization, FVM modeling.*

Introduction

The continuous drive toward higher performance, increased integration density, and miniaturization in semiconductor devices has positioned flip-chip technology as a foundational architecture in modern electronic packaging. Compared with conventional wire bonding, flip-chip interconnection offers reduced signal inductance, improved thermal dissipation, shorter electrical paths, and higher input/output (I/O) density, making it particularly suitable for high-speed computing, mobile electronics, and IoT applications (Apalowo et al., 2024a; Apalowo et al., 2025; Hung et al., 2024). Despite these advantages, mechanical reliability remains a critical concern due to thermo-mechanical stresses induced by coefficient of thermal expansion (CTE) mismatch between the silicon die and the organic substrate. Underfill encapsulation is therefore an essential post-assembly process in flip-chip packaging. By dispensing a capillary-driven polymeric resin into the narrow gap between the die and substrate, underfill redistributes stresses away from solder joints, thereby mitigating fatigue damage and enhancing long-term reliability (Apalowo et al., 2026a; Apalowo et al., 2024b). However, the effectiveness of this process depends strongly on the dynamics of resin infiltration.

A key performance metric in underfill encapsulation is flow time, defined as the duration required for the resin to wet and substantially fill the interconnect gap beneath the die (Ng et al., 2018; Stencel et al., 2023). Flow time directly influences manufacturing throughput, wetting uniformity, and the probability

of void formation, which can compromise mechanical integrity and lead to premature package failure (Wang et al., 2019). The capillary-driven flow process is governed by a coupled interaction among underfill viscosity, surface tension, contact angle, solder bump geometry, and dispensing strategy (Wan et al., 2005; Zhou & Sun, 2012). For instance, concave and hourglass-shaped solder bumps can facilitate streamlined capillary pathways, whereas spherical or cylindrical geometries may introduce local flow resistance and increase encapsulation time (Hung et al., 2024).

Dispensing configuration further modulates flow behavior. Injection layouts such as in-line and multi-inlet (ILU-type) strategies determine pressure distribution and front propagation symmetry. Imbalanced flow partitioning may induce racing effects, backflow, and air entrapment, thereby prolonging filling time and increasing defect susceptibility (Khor et al., 2010). Additionally, underfill materials often exhibit high filler loading and non-Newtonian characteristics, introducing further nonlinearities into the flow field (Wang et al., 2019). Traditional analytical formulations, typically derived under assumptions of steady laminar flow, constant contact angle, and idealized geometries, struggle to accurately capture these coupled Multiphysics interactions (Lee et al., 2008; Wan et al., 2005).

To address these limitations, machine learning (ML) approaches have emerged as powerful data-driven tools for modeling complex nonlinear systems. Unlike purely physics-based models, ML algorithms infer functional relationships directly from data, enabling high-dimensional mapping between process parameters and performance metrics without explicit constitutive simplifications (Jordan & Mitchell, 2015; Schmidhuber, 2015). In microelectronic packaging, ML techniques have been successfully applied to predict void formation, thermal stresses, and encapsulation uniformity (Apalowo et al., 2026b; Stencel et al., 2023).

Among available algorithms, ensemble-based methods such as Random Forest and XGBoost demonstrate strong robustness for structured datasets containing mixed categorical and continuous variables, while Artificial Neural Networks (ANNs) provide flexible nonlinear function approximation capabilities when sufficient data are available (Breiman, 2001; Chen & Guestrin, 2016; Lecun et al., 2015). When trained on high-fidelity simulation outputs, these models can learn intricate dependencies between dispensing configuration, solder bump geometry, underfill properties, and resulting flow time (Akiba et al., 2019). Furthermore, Bayesian optimization frameworks such as Optuna and Scikit-Optimize enable efficient hyperparameter tuning through probabilistic search strategies, outperforming conventional grid or random search in limited-data regimes (Bergstra & Bengio, 2012).

Recent studies have increasingly integrated Computational Fluid Dynamics (CFD) simulations with ML-based surrogate modeling to reduce computational cost while preserving predictive fidelity (Stencel et al., 2023). Building upon this paradigm, the present work develops a hybrid CFD–ML framework to optimize and predict underfill flow time in flip-chip BGA encapsulation. The objective is to provide a physics-informed, data-driven decision support tool capable of reducing process cycle time, enhancing encapsulation reliability, and accelerating virtual prototyping in advanced microelectronic manufacturing.

Methodology

This study adopts a hybrid physics-based and data-driven framework to investigate and optimize underfill flow time in flip-chip encapsulation. Three primary process variables were considered: dispensing methodology, solder bump geometry, and underfill material properties. The methodology integrates high-fidelity Computational Fluid Dynamics (CFD) simulations performed in ANSYS Fluent with Taguchi parametric analysis and machine learning (ML) modeling for process optimization and predictive surrogate development.

A total of 120 simulation cases were generated to capture all combinations of the selected factors. The resulting dataset was subsequently used for statistical analysis, optimization, and ML-based regression modeling.

Numerical Simulation

Geometric Model

The computational model represents a flip-chip package consisting of a silicon die, PCB substrate, solder bump array, and fluid domain (encapsulation gap). A 10 × 10 Ball Grid Array (100 solder joints) was embedded between the die and substrate to emulate realistic interconnect configuration and capture flow behavior within a dense bump array.

The geometric dimensions of the package components are summarized in Table 1.

Table 1: Dimensions of the flip-chip package components

Component	Dimensions (mm^3)
PCB Substrate	14 × 14 × 1
Silicon Die	10.5 × 10.5 × 1
Fluid Domain	10.5× 10.5 × 0.45

The fluid domain thickness (0.45 mm) corresponds to the standoff height between the die and substrate. The complete three-dimensional model developed in ANSYS Fluent is illustrated in Figure 1. The complete three-dimensional model developed in ANSYS Fluent is illustrated in Figure 1, where Figure 1(a) shows the assembled flip-chip package structure and Figure 1(b) highlights the solder bump array embedded between the die and PCB substrate.

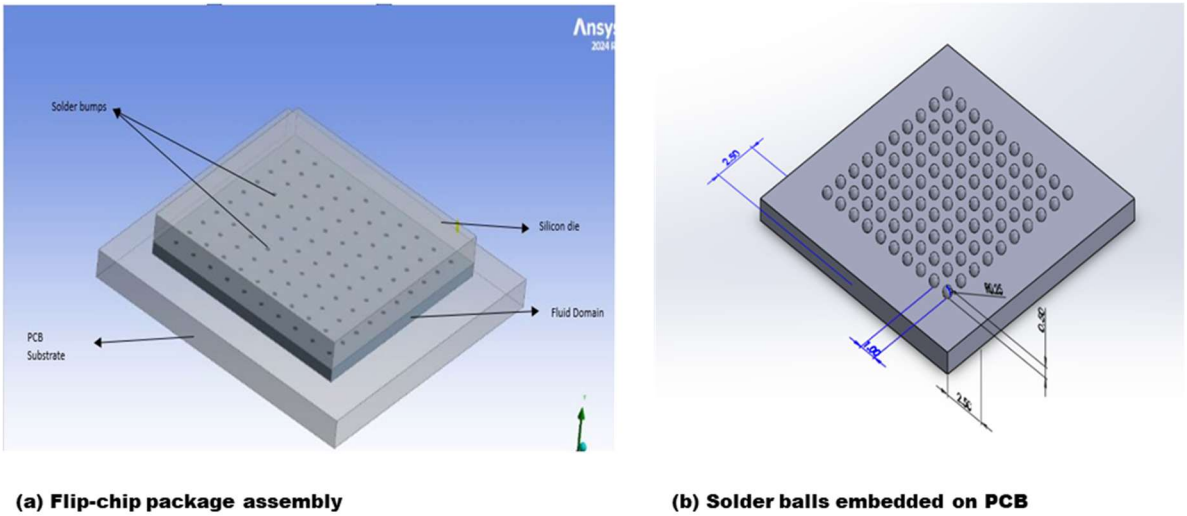

(a) Flip-chip package assembly **(b) Solder balls embedded on PCB**

Figure 1: Three-dimensional geometric model of the flip-chip Ball Grid Array (BGA) package used for underfill flow simulation

Solder Bump Geometry

Four solder bump geometries were evaluated, namely spherical, cylindrical, hourglass, and concave.

To isolate geometric effects from volumetric influence, each bump was designed to maintain identical volume (0.0645 mm^3) and pitch (1.0 mm). This ensured constant porosity within the interconnect region across all simulations, allowing flow behavior to be attributed solely to geometric curvature and surface morphology rather than size variation.

Key geometric parameters are summarized in Table 2.

Table 2: Physical properties of the underfill material used in the simulation, governing capillary-driven flow behavior during flip-chip encapsulation

Parameters of solder bump	Dimensions of actual-sized solder bump in 10 × 10 full array flip-chip			
	Spherical	Cylindrical	Hourglass	Concave
Spherical diameter, d_s (mm)	0.5	-	0.5	-
Pitch (mm)	1.0	1.0	1.0	1.0
Gap height, h (mm)	0.45	0.45	0.45	0.45
Volume of single bump (mm^3)	0.0645	0.0645	0.0645	0.0645

Table 3: Thermophysical properties of the underfill material used in the numerical simulations (Hassan et al., 2023)

Material	Viscosity [Pa·s]	Surface Tension [N/m]	Density [kg/m³]
30% Methanol/DI	0.0018	0.032	958.2
20% Ethanol/DI	0.0022	0.034	970.4
50% Ethylene Glycol/DI	0.0200	0.027	1070.0
50% Glycerol/DI	0.0400	0.030	1110.0
100% Glycerol	1.2000	0.0634	1261.0

Underfill Material Properties

Five underfill materials were selected to span a wide rheological spectrum. These aqueous mixtures of methanol, ethanol, ethylene glycol, and glycerol were chosen based on differences in dynamic viscosity, surface tension, and density. The material properties used in the computational models are summarized in Table 3.

The viscosity range (0.0018-1.2 Pa·s) enabled simulation of both low-resistance and highly viscous flow regimes. This broad property space enhances model generalization capability and enables robust ML training.

Dispensing Configurations

Six dispensing configurations were investigated: I-100 (single inlet, 100%), L-50 (two inlets, 50/50), L-60 (60/40), L-75 (75/25), U-33.3 (three inlets, equal split), and U-40 (40/30/30).

These configurations represent practical dispensing approaches employed in semiconductor packaging to minimize void formation and improve encapsulation efficiency. The dispensing methods considered in this work are summarized in Table 4.

A key methodological contribution of this work is the implementation of an inlet-area-balanced dispensing strategy. Unlike prior studies that allowed variations in total inlet area among configurations, this approach maintained a constant total inlet cross-sectional area for all cases. This ensures that differences in flow time arise from pressure distribution and flow dynamics rather than volumetric injection bias, thereby improving the internal validity of comparative analysis.

Table 4: Underfill dispensing configurations evaluated in the CFD simulations for the flip-chip BGA encapsulation process.

Dispensing method	Number of inlet	Inlet split by percentage (%)	Visual Representation
I-100	1	100	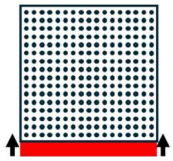
L-50	2	50, 50	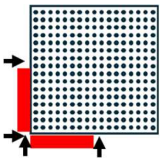
L-60	2	60, 40	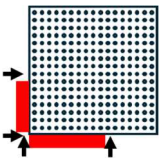
L-75	2	75, 25	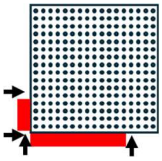
U-33.3	3	33.3, 33.3, 33.3	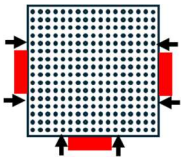
U-40	3	40, 30, 30	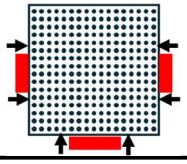

Mesh Generation and Boundary Conditions

The fluid domain was discretized using the automated meshing tool in ANSYS Fluent, generating high-resolution structured hexahedral elements suitable for narrow-gap and multiphase flow simulations.

Boundary conditions were defined as follows:

- No-slip condition at all solid walls
- Static contact angle of 30°
- Atmospheric pressure at outlets
- Inlet velocity distribution defined according to dispensing configuration

Multiphase interaction between underfill and displaced air was modeled dynamically during encapsulation.

Governing Equations

Underfill infiltration was modeled as an unsteady, laminar, incompressible multiphase flow governed by the continuity, momentum, and Volume of Fluid (VOF) equations.

The continuity equation is crucial for mass conservation in the simulation. It is expressed as:

$$\frac{\partial \rho}{\partial t} + \nabla \cdot (\rho \vec{u}) = 0 \quad (1)$$

where ρ represents the fluid density and $\vec{u}$ denotes the velocity vector.

Furthermore, the conservation of momentum within the fluid is described by the momentum equation, also known as the Navier-Stokes equation. It is described as:

$$\frac{\partial}{\partial t}(\rho \vec{u}) + \nabla \cdot (\rho \vec{u} \cdot \vec{u}) = -\nabla p + \nabla \tau + \rho \vec{g} \quad (2)$$

where p denotes the pressure, τ is the dynamic viscosity, and $\vec{g}$ represents the gravitational acceleration vector. Finally, the Volume of Fluid (VOF) equation is given as:

$$\frac{\partial \alpha}{\partial t} + \vec{u} \cdot (\nabla \alpha) = 0 \quad (3)$$

where α is the volume fraction of underfill ($0 \leq \alpha \leq 1$). This formulation enables accurate interface tracking between air and underfill during capillary-driven infiltration.

Taguchi Analysis and Machine Learning Modeling

This study involved 120 simulation runs, covering combinations of five underfill materials, four solder bump geometries, and six dispensing configurations.

Taguchi design of experiments (DOE) was first applied to quantify main and interaction effects of process parameters on flow time. Subsequently, machine learning models were developed to construct predictive surrogate models.

Three regression algorithms were evaluated: Random Forest Regressor, XGBoost Regressor, and Artificial Neural Network (ANN). The objective was to determine the most accurate model for predicting encapsulation time based on combined solder bump shapes, underfill materials, and dispensing configurations.

Results and Discussion

Underfill Flow Progression

Table 5 presents a graphical representation of the underfill filling progression obtained from the simulations using methanol as the underfill material across all dispensing methods and solder bump geometries. The filling patterns are shown at 25%, 50%, 75%, and 95% completion levels of the fluid domain.

The results show that the initial flow behavior differs depending on the dispensing configuration, primarily due to variations in the direction and distribution of capillary pressure gradients. However, as the filling process progresses, the I and U dispensing methods exhibit similar convergence characteristics near the final stages of encapsulation.

This convergence suggests that U-type dispensing configurations facilitate more balanced flow propagation across the fluid domain, which can reduce the likelihood of air entrapment and void formation during the encapsulation process. This characteristic aligns with the design objective of multi-directional underfill delivery, where the fluid front advances simultaneously from multiple directions, thereby minimizing stagnation zones.

An important observation from the simulations is that complete filling of the fluid domain (100%) was not achieved in the simulation environment due to the presence of residual microvoids and trapped air pockets. Consequently, 95% filling of the fluid domain was adopted as the standardized upper threshold for measuring encapsulation time. This approach is consistent with common practices in underfill process simulation where near-complete

filling is considered representative of practical manufacturing conditions.

Table 5: Simulated underfill filling progression for different dispensing configurations and solder bump geometries using methanol as the underfill material

Fill Progression	25 %	50 %	75 %	95 %
I-100	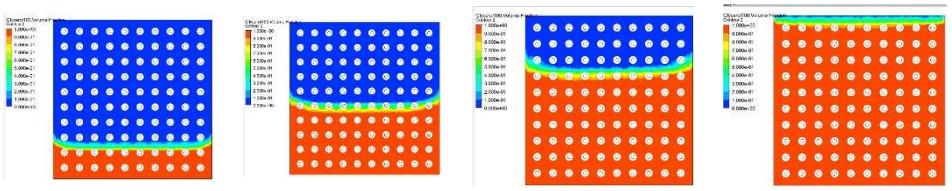			
L-50	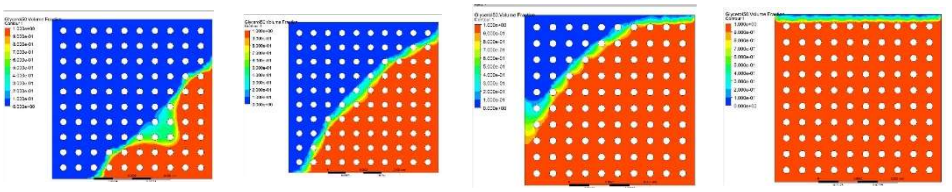			
L-60	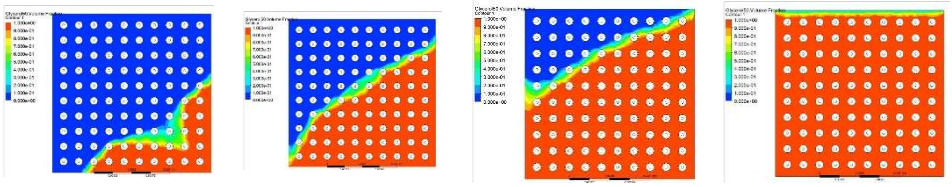			
L-75	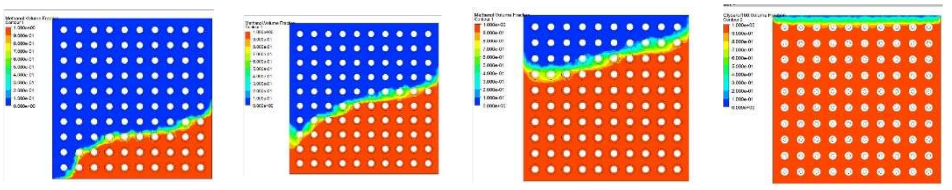			
U-40	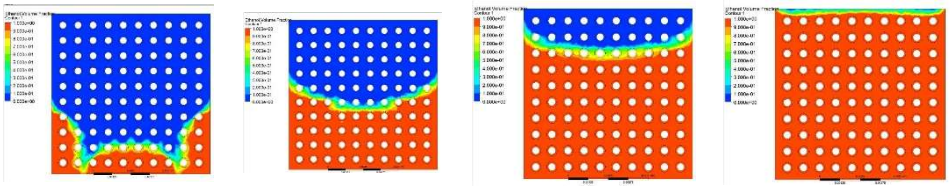			
U-33	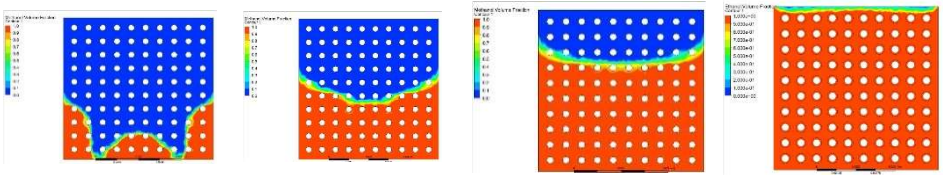			

Parametric Study Using Taguchi Analysis

The objective of the parametric analysis was to identify dominant process variables and establish baseline relationships between material properties, geometric parameters, and dispensing strategies.

Main Effects Analysis

The main effects analysis reveals a clear hierarchical influence among the three investigated parameters. Figure 2 presents the Taguchi main effects plot for fill time, illustrating the independent influence of each factor on the encapsulation process.

Among the investigated variables, underfill material properties emerge as the most dominant factor influencing flow time. This variation is primarily governed by differences in viscosity, surface

tension, and density, which collectively determine capillary-driven flow behavior within the narrow die–substrate gap.

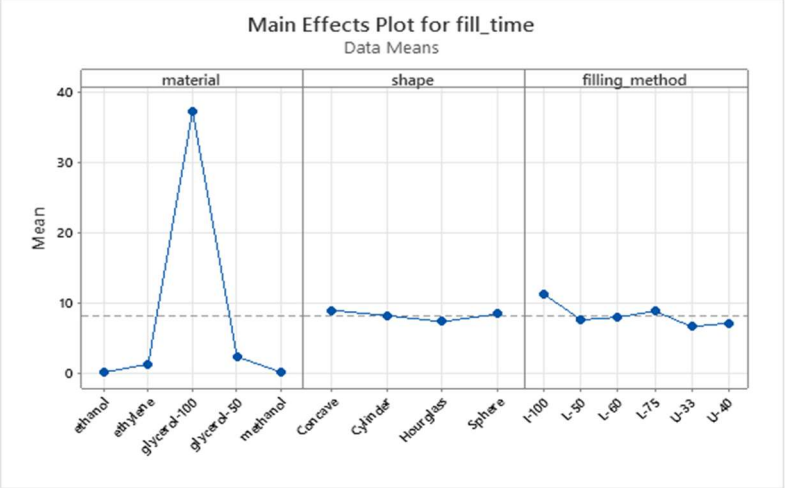

Figure 2: Taguchi main effects plot illustrating the influence of underfill material properties, solder bump geometry, and dispensing configuration on underfill flow time

From the main effects plot, Glycerol-100 exhibits the highest average fill time of approximately 38 seconds, which is more than 300 times greater than the lowest recorded fill times. This behavior is attributed to its high viscosity (1.20 Pa·s), which introduces substantial resistance to flow within the micro-scale interconnect structure. In contrast, methanol and ethanol exhibit the shortest fill times, corresponding to viscosities of 0.0018 Pa·s and 0.0022 Pa·s, respectively. These materials possess favorable rheological and wetting characteristics, enabling rapid capillary propagation of the underfill front. Notably, methanol consistently achieved the lowest flow time across most configurations, confirming its suitability as a low-viscosity underfill candidate for high-throughput manufacturing environments where encapsulation cycle time is critical.

The dispensing configuration demonstrated a moderate but significant effect on flow time. Among the investigated configurations, U-33.3 multi-inlet dispensing produced the lowest average fill time (6.63 s) and I-100 single-inlet dispensing produced the highest average fill time (~11 s). Similarly, within the L-type configurations, L-50 outperformed both L-60 and L-75, highlighting the importance of balanced inlet distribution and reduced flow path asymmetry.

Solder bump geometry exhibited only a marginal influence on flow time within the investigated parameter range. The hourglass bump geometry recorded the lowest mean fill time (7.35 s), followed by cylinder (8.2 s), spherical (8.5 s), and concave (~9 s). However, these differences were relatively small and statistically insignificant. Consequently, bump geometry optimization alone is unlikely to produce substantial improvements in encapsulation performance, unless combined with low-viscosity underfill materials and optimized dispensing strategies.

Interaction Effects Between Process Parameters

While the main effects analysis provides insight into individual factor contributions, it does not capture the combined influence of interacting variables. To address this limitation, interaction plots derived from the Taguchi design were used to analyze cross-factor dependencies and synergistic effects.

Figure 3 illustrates the interaction between underfill material type and dispensing strategy. The plot reveals a strong interaction effect for highly viscous materials. For Glycerol-100, the fill time varies significantly across dispensing methods, ranging from over 52 seconds for I-100 to approximately 30 seconds for U-33 and U-40. This steep slope indicates that flow performance for highly viscous fluids is strongly dependent on dispensing strategy. Conversely, methanol, ethanol, ethylene glycol, and glycerol-50 consistently exhibit low fill times regardless of dispensing configuration. Their clustering near the bottom of the graph suggests that dispensing method has minimal influence when

low-viscosity materials are used. Multi-inlet configurations such as U-33 introduce distributed pressure gradients, promoting faster and more uniform flow front propagation. For high-viscosity underfills, however, dispensing strategy must be co-optimized with material properties to overcome viscous resistance. In such cases, tri-directional strategies such as U-33 and U-40 significantly reduce flow time compared with single-inlet configurations.

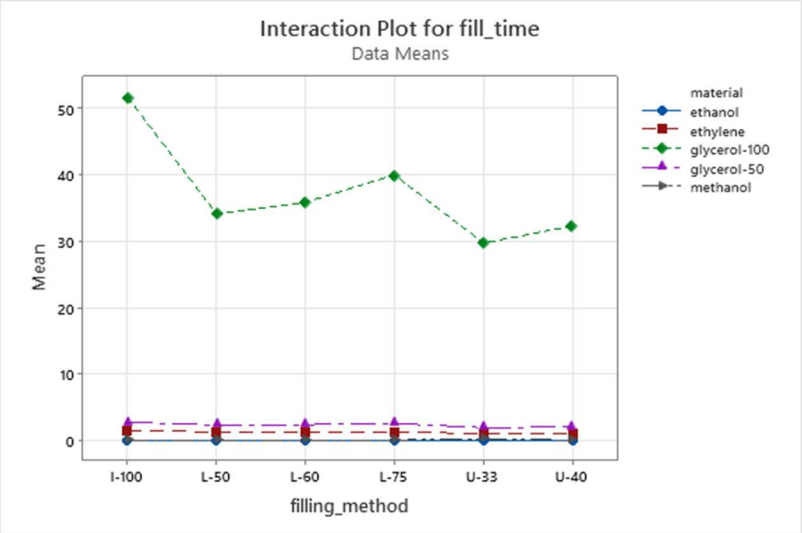

Figure 3: Interaction plot showing the combined effect of underfill material type and dispensing method on underfill flow time

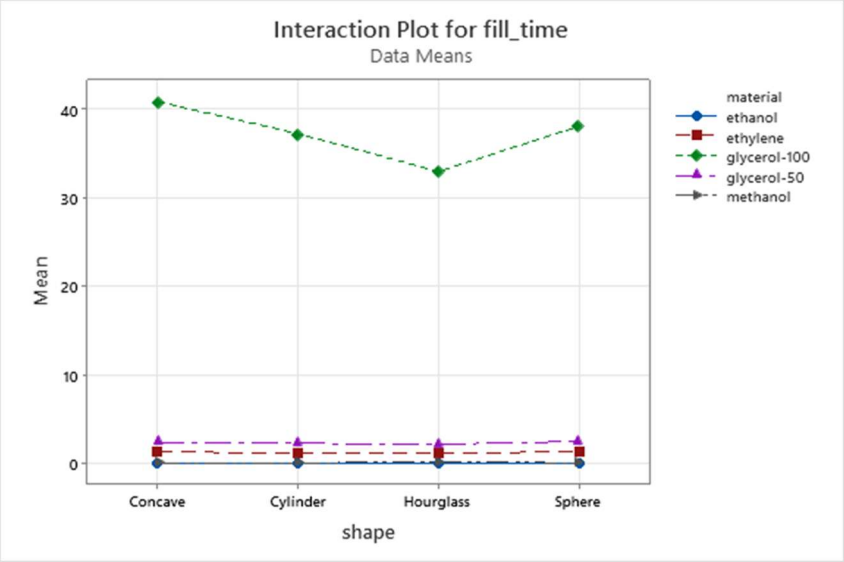

Figure 4: Interaction plot illustrating the influence of solder bump geometry and dispensing method on underfill flow time

Figure 4 presents the interaction between solder bump geometry and dispensing strategy. Although less pronounced than material interactions, a clear pattern can still be observed. The concave bump geometry combined with the I-100 dispensing method produces the highest fill time (~14.5 s). However, when paired with the U-33 dispensing configuration, the fill time drops sharply to below 7

seconds. This trend is consistent across all bump geometries, demonstrating that single-inlet dispensing configurations generally produce slower encapsulation compared with multi-inlet approaches. Across nearly all geometries, U-33 consistently produces the fastest underfill propagation, highlighting its effectiveness in reducing flow path resistance and promoting uniform capillary advancement. Unlike the interaction observed in Figure 3, this plot indicates that bump shape and dispensing configuration can exert noticeable influence on flow behavior when material properties remain constant.

The interaction plot between underfill material and solder bump geometry is shown in Figure 5. The observed trends are similar to those presented in the material–dispensing interaction plot, further confirming that material viscosity dominates underfill flow behavior. For Glycerol-100, bump geometry significantly affects fill time, with hourglass having a fill time of ~33 s, cylinder and sphere within 36–38 s, and concave greater than 41 s. This indicates that geometric variations can influence capillary resistance when viscous fluids are used. In such conditions, optimizing bump profile can reduce flow tortuosity and improve encapsulation efficiency. In contrast, for Methanol, Ethanol, and Ethylene, fill times remain consistently low across all bump geometries. The high mobility of these fluids minimizes geometric effects, allowing greater design flexibility in bump shape selection.

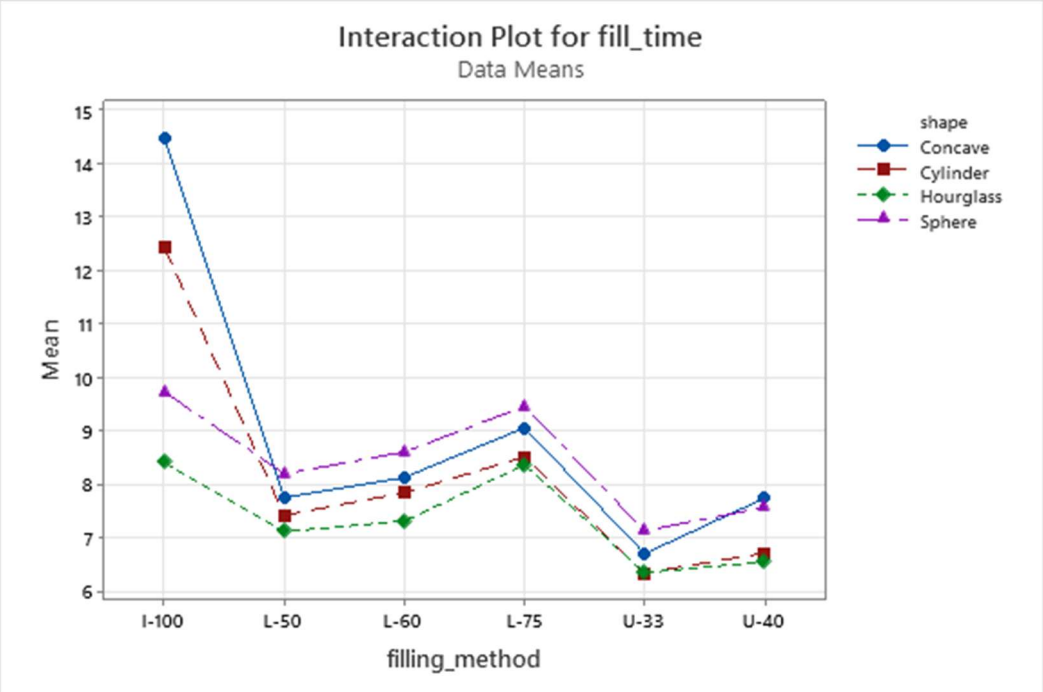

Figure 5: Interaction plot depicting the relationship between underfill material properties and solder bump geometry

Machine Learning Optimization and Prediction

Optimization Algorithms and Tools

To identify the optimal process parameters for minimizing underfill flow time, two Bayesian optimization frameworks were employed: Tree-structured Parzen Estimator (TPE) using the Optuna optimization library and Gaussian Process Regression (GPR) using the Scikit-optimize library. Both algorithms were used to explore the parameter space and determine optimal configurations over 100 optimization trials. The resulting convergence histories are presented in Figures 6 and 7. Both optimization approaches converged toward a similar optimal configuration, indicating stable parameter search and consistent model behavior.

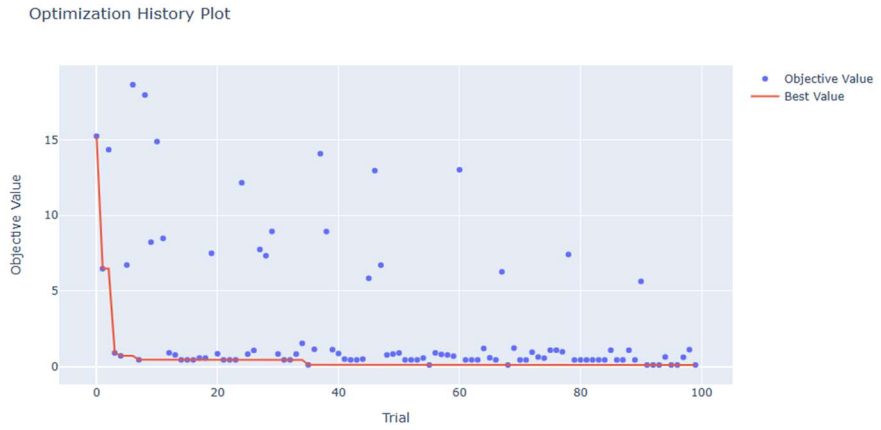

Figure 6: Convergence history plot obtained using the Scikit-optimize Bayesian optimization framework

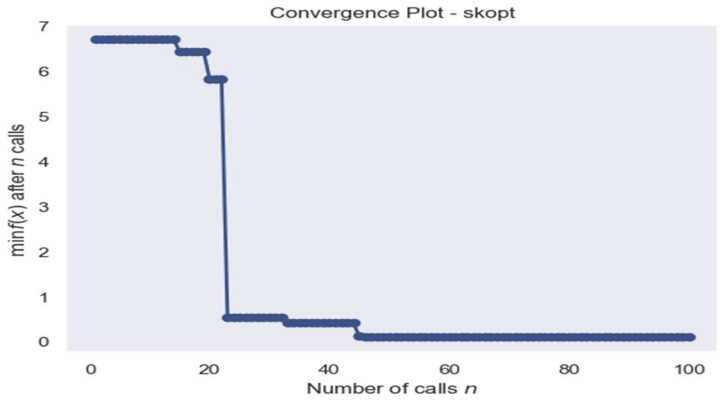

Figure 7: Optimization history plot generated using the Optuna Tree-structured Parzen Estimator (TPE) algorith

Table 6: Optimal process parameter combination identified through Bayesian optimization for minimizing underfill encapsulation flow time

Parameter	Optimal Value
Solder Ball Shape	Hourglass
Dispensing Method	U-33.3
Viscosity	0.0018 Pa·s
Surface Tension	44.42 N/m
Density	958.2 kg/m^3

The optimal configuration identified by the optimization algorithms is summarized in Table 6, which aligns closely with observations from the Taguchi parametric analysis.

Machine Learning Models and Evaluation

Three machine learning models were evaluated for predicting underfill flow time. These models include Random Forest Regressor, XGBoost Regressor, and Artificial Neural Network (ANN). Model performance was assessed using Root Mean Square Error (RMSE). The RMSE measures the average magnitude of prediction errors between model outputs and simulation results, providing a quantitative indicator of prediction accuracy. The evaluation results are summarized in Table 7.

Table 7. Performance comparison of machine learning models

Model	RMSE	Performance Ranking
Random Forest	1.19	1st
XGBoost	1.22	2nd
ANN	2.88	3rd

The Random Forest model achieved the lowest RMSE, indicating the highest predictive accuracy. Its ensemble tree-based architecture enables effective modeling of nonlinear relationships between categorical and continuous variables, making it well suited for the heterogeneous dataset used in this study.

Predictive Performance and Visualization

The predictive performance of the selected model was further evaluated by comparing predicted flow times with simulation values, as shown in Figure 8.

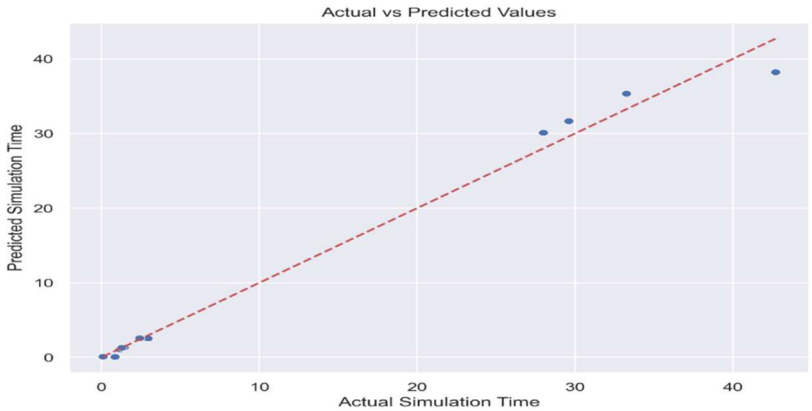

Figure 8: Comparison of Random Forest predicted flow times and simulation results showing the correlation between model predictions and CFD simulation data

The prediction plot shows strong correlation between predicted and actual values, with most predictions closely following the ideal trend line. This indicates that the Random Forest model successfully learned the underlying relationships between process parameters and underfill flow time. However, it can also be observed that many predicted values cluster near the extreme regions of the plot, suggesting that the training dataset contained limited intermediate samples. This indicates that additional simulation data covering a wider range of parameter combinations could further improve model generalization and prediction accuracy.

Conclusion

This study investigated the optimization and prediction of underfill flow time during flip-chip Ball Grid Array (BGA) encapsulation by integrating computational fluid dynamics (CFD) simulations with machine learning–based predictive modeling. The primary objective was to understand the influence of underfill material properties, solder bump geometries, and dispensing configurations on capillary-driven flow behavior and to develop a data-driven framework capable of predicting and minimizing encapsulation time.

A comprehensive parametric study was first conducted using a Taguchi experimental design based on 120 CFD simulation cases covering five underfill materials, four solder bump shapes, and six dispensing strategies. The results demonstrated that underfill material properties, particularly viscosity, are the dominant factors governing flow behavior. Highly viscous materials such as glycerol-100 produced significantly longer fill times, whereas low-viscosity fluids such as methanol and ethanol enabled rapid capillary propagation and substantially reduced encapsulation time. Dispensing strategy was identified as the second most influential factor, with the multi-inlet U-33.3 configuration consistently producing the fastest filling performance. In contrast, solder bump geometry showed only marginal influence within the investigated parameter range.

Interaction analysis further revealed that dispensing configuration becomes increasingly critical when high-viscosity materials are used, highlighting the importance of co-optimizing material selection and dispensing design to overcome viscous resistance. Bayesian optimization using Optuna and Scikit-optimize identified the optimal process configuration as the combination of hourglass bump geometry, U-33.3 dispensing method, and low-

viscosity underfill properties (0.0018 Pa·s). For predictive modeling, three machine learning algorithms, Random Forest, XGBoost, and Artificial Neural Networks, were evaluated. The Random Forest model achieved the highest predictive accuracy with the lowest root mean square error (RMSE) of 1.19, demonstrating strong capability in capturing nonlinear interactions between process variables.

Overall, this study presents a scalable hybrid framework combining CFD simulation, statistical design, and machine learning to accelerate process optimization in flip-chip encapsulation. The findings provide practical guidance for semiconductor packaging engineers seeking to reduce encapsulation cycle time, minimize void formation, and improve manufacturing throughput. Furthermore, the developed predictive approach offers a foundation for intelligent process design and virtual prototyping in advanced electronic packaging systems.

References

Akiba, T., Sano, S., Yanase, T., Ohta, T., & Koyama, M. (2019). Optuna: A Next-generation Hyperparameter Optimization Framework. *Proceedings of the ACM SIGKDD International Conference on Knowledge Discovery and Data Mining*, 2623–2631. https://doi.org/10.1145/3292500.3330701

Apalowo, R. K., Abas, A., Bin Salim, M. R., Famuyiwa, S. O., & Kok, C. S. (2026). Heat dissipation performance of solid-state drives under convective cooling: analyzing the impact of heat sink fin spacing. *Microelectronics International*, 1–16. https://doi.org/10.1108/MI-03-2025-0044

Apalowo, R. K., Abas, M. A., Bachok, Z., Sharif, M. F. M., Che Ani, F., Ramli, M. R., & Mukhtar, M. A. F. bin M. (2024). Deformation and crack growth in multilayered ceramic capacitor during thermal reflow process: numerical and experimental investigation. *Microelectronics International*, *41*(3), 162–171. https://doi.org/10.1108/MI-03-2023-0025/FULL/XML

Apalowo, R. K., Abas, M. A., Mukhtar, M. A. F. M., & Ramli, M. R. (2025). Investigation of the Impacts of Solder Alloy Composition and Temperature Profile on Fatigue Life of Ball Grid Array Solder Joints Under Accelerated Thermal Cycling. *Journal of Electronic Packaging*, *147*(1). https://doi.org/10.1115/1.4065805

Apalowo, R. K., Kareem, A., Ikudehinbu, E., Somefun, D., Ukpoweh, G., Kehinde, E., & Oyeleke, E. (2026). Data-Driven Optimization of Nanoparticle-Reinforced Underfill Encapsulation in Ball Grid Array (BGA) Assemblies. *Journal of Metastable and Nanocrystalline Materials*, *43*, 17–28. https://doi.org/10.4028/p-isii0y

Apalowo, R. K., Muhamed Mukhtar, M. A. F., Abas, M. A., & Che Ani, F. (2024). Numerical modeling and optimization of fillet height of reinforced SAC305 solder joint in an ultra-fine capacitor assembly. *Soldering & Surface Mount Technology*, *36*(5), 309–322. https://doi.org/10.1108/SSMT-04-2024-0020

Bergstra, J., & Bengio, Y. (2012). Random search for hyper-parameter optimization. *The Journal of Machine Learning Research*. https://doi.org/10.5555/2188385.2188395

Breiman, L. (2001). Random forests. *Machine Learning*, *45*(1), 5–32. https://doi.org/10.1023/A:1010933404324

Chen, T., & Guestrin, C. (2016). XGBoost: A scalable tree boosting system. *Proceedings of the ACM SIGKDD International Conference on Knowledge Discovery and Data Mining*, *13-17-August-2016*, 785–794. https://doi.org/10.1145/2939672.2939785

Hassan, R. U., Khalil, S. M., Khan, S. A., Moon, J., Cho, D. H., & Byun, D. (2023). Electric field and viscous fluid polarity effects on capillary-driven flow dynamics between parallel plates. *Heliyon*, *9*(6). https://doi.org/10.1016/j.heliyon.2023.e16395

Hung, H.-H., Cheng, Y.-C., Hwang, S.-J., Chen, D.-L., Chang, H.-J., Huang, B.-Y., Huang, H.-H., Wang, C.-C., & Hung, C.-P. (2024). Analysis of flip-chip ball grid array underfill flow process. *The International Journal of Advanced Manufacturing Technology 2024 134:9*, *134*(9), 4851–4870. https://doi.org/10.1007/S00170-024-14304-1

Jordan, M. I., & Mitchell, T. M. (2015). Machine learning: Trends, perspectives, and prospects. *Science*, *349*(6245), 255–260. https://doi.org/10.1126/science.aaa8415

Khor, C. Y., Abdul Mujeebu, M., Abdullah, M. Z., & Che Ani, F. (2010). Finite volume based CFD simulation of pressurized flip-chip underfill encapsulation process. *Microelectronics Reliability*, *50*(1), 98–105. https://doi.org/10.1016/j.microrel.2009.08.007

Lecun, Y., Bengio, Y., & Hinton, G. (2015). Deep learning. *Nature*, *521*(7553), 436–444. https://doi.org/10.1038/nature14539

Lee, S., Yim, M. J., Master, R. N., Wong, C. P., & Baldwin, D. F. (2008). Void formation study of flip chip in package using no-flow underfill. *IEEE Transactions on Electronics Packaging Manufacturing*, *31*(4), 297–305. https://doi.org/10.1109/TEPM.2008.2002951

Ng, F. C., Abas, A., & Abdullah, M. Z. (2018). Effect of solder bump shapes on underfill flow in flip-chip encapsulation using analytical, numerical and PIV experimental approaches. *Microelectronics Reliability*, *81*, 41–63. https://doi.org/10.1016/J.MICROREL.2017.12.025

Schmidhuber, J. (2015). Deep learning in neural networks: An overview. *Neural Networks*, *61*, 85–117. https://doi.org/10.1016/j.neunet.2014.09.003

Stencel, L. C., Strogies, J., Müller, B., Knofe, R., Borwieck, C., & Heimann, M. (2023). Capillary Underfill Flow Simulation as a Design Tool for Flow-Optimized Encapsulation in Heterogenous Integration. *Micromachines 2023, Vol. 14, Page 1885*, *14*(10), 1885. https://doi.org/10.3390/MI14101885

Wan, J. W., Zhang, W. J., & Bergstrom, D. J. (2005). Influence of transient flow and solder bump resistance on underfill process. *Microelectronics Journal*, *36*(8), 687–693. https://doi.org/10.1016/j.mejo.2005.05.022

Wang, H., Su, Y., Wang, W., Sheng, G., Li, H., & Zafar, A. (2019). Enhanced water flow and apparent viscosity model considering wettability and shape effects. *Fuel*, *253*, 1351–1360. https://doi.org/10.1016/j.fuel.2019.05.098

Zhou, S., & Sun, Y. (2012). Multiscale, multiphysics model of underfill flow for flip-chip packages. *IEEE Transactions on Components, Packaging and Manufacturing Technology*, *2*(6), 893–902. https://doi.org/10.1109/TCPMT.2012.2184762